



Article

Cite this article: Guillet G, Preunkert S, Ravanel L, Montagnat M, Friedrich R (2021). Investigation of a cold-based ice apron on a high-mountain permafrost rock wall using ice texture analysis and micro-¹⁴C dating: a case study of the Triangle du Tacul ice apron (Mont Blanc massif, France). *Journal of Glaciology* **67**(266), 1205–1212. <https://doi.org/10.1017/jog.2021.65>

Received: 21 April 2020

Revised: 17 May 2021

Accepted: 18 May 2021

First published online: 10 June 2021

Keywords:

Ice chronology/dating; ice core; ice crystal studies; mountain glaciers

Author for correspondence:

Grégoire Guillet,

E-mail: gregoire.guillet@univ-smb.fr

Investigation of a cold-based ice apron on a high-mountain permafrost rock wall using ice texture analysis and micro-¹⁴C dating: a case study of the Triangle du Tacul ice apron (Mont Blanc massif, France)

Grégoire Guillet^{1,2} , Susanne Preunkert³, Ludovic Ravanel¹,
Maurine Montagnat^{3,4}  and Ronny Friedrich⁵

¹EDYTEM, Univ. Savoie Mont-Blanc, Univ. Grenoble Alpes/CNRS, Chambéry, France; ²School of Geography and Sustainable Development, University of St Andrews, St Andrews, UK; ³Univ. Grenoble Alpes, CNRS, IRD, IGE, F-38000 Grenoble, France; ⁴Univ. Grenoble Alpes, Univ. de Toulouse, Météo-France, CNRS, CNRM, Centre d'Études de la Neige, Grenoble, France and ⁵Curt-Engelhorn-Center Archaeometry, Mannheim, Germany

Abstract

The current paper studies the dynamics and age of the Triangle du Tacul (TDT) ice apron, a massive ice volume lying on a steep high-mountain rock wall in the French side of the Mont-Blanc massif at an altitude close to 3640 m a.s.l. Three 60 cm long ice cores were drilled to bedrock (i.e. the rock wall) in 2018 and 2019 at the TDT ice apron. Texture (microstructure and lattice-preferred orientation, LPO) analyses were performed on one core. The two remaining cores were used for radiocarbon dating of the particulate organic carbon fraction (three samples in total). Microstructure and LPO do not substantially vary with along the axis of the ice core. Throughout the core, irregularly shaped grains, associated with strain-induced grain boundary migration and strong single maximum LPO, were observed. Measurements indicate that at the TDT ice deforms under a low strain-rate simple shear regime, with a shear plane parallel to the surface slope of the ice apron. Dynamic recrystallization stands out as the major mechanism for grain growth. Micro-radiocarbon dating indicates that the TDT ice becomes older with depth perpendicular to the ice surface. We observed ice ages older than 600 year BP and at the base of the lowest 30 cm older than 3000 years.

1. Introduction

Ice aprons, also known as ice faces (Gruber and Haeberli, 2007; Hasler and others, 2011), are scarce accumulations of massive ice found in glacierized basins, above the equilibrium line (Armstrong and Roberts, 1956; Bhutiyani, 2011; Cogley and others, 2011; Guillet and Ravanel, 2020). Such a definition typically encompasses ice masses from different settings like isolated massive ice patches on rock walls (e.g. north face of Mount Alberta, Canadian Rocky Mountains) or any steep ice body lying over a glacial bergschrund, defined by Cogley and others (2011) as ‘a crevasse at the head of a glacier that separates flowing ice from stagnant ice, or from a rock headwall’ (e.g. the Triangle du Tacul ice apron, Mont-Blanc massif, cf. Section 2.1, see Guillet and Ravanel (2020) for more details).

Unlike other cryospheric objects, most notably large valley and cirque glaciers, ice aprons received little attention from the scientific community until now. Due to their small spatial extent (typically ranging between 0.01 and 0.1 km²) compared to other glaciers, ice aprons are not expected to have a significant impact on water resource availability. However, in populated mountainous regions relying heavily on the high mountain environment for recreation and tourism like the Chamonix valley (Barker, 1982; Hall and Higham, 2005), the shrinkage of ice aprons raises concerns. Glacial recession and thermal destabilization of the permafrost have been identified as important factors for the recent increase in high mountain rock wall instabilities (Huggel and others, 2012; Ravanel and others, 2013; Deline and others, 2021). Ice aprons, covering steep rock walls, protect the underlying permafrost from thawing. Reduction in their surface area or complete disappearance would thus accelerate the ongoing destabilization of rock walls (Gruber and Haeberli, 2007; Kenner and others, 2011; Guillet and Ravanel, 2020). In addition, in the Mont-Blanc massif (MBM; France), ice aprons are often mandatory passing points for most classical mountaineering routes, existing since the beginning of alpinism in Europe in the 18th century (Mourey and others, 2019). The disintegration of ice aprons would therefore also lead to an important loss in European alpine culture heritage.

In a companion paper, focused on the surface area variations of ice aprons in the MBM, Guillet and Ravanel (2020) showed that ice aprons have been losing mass since the end of the Little Ice Age (LIA), with accelerated shrinkage since the 1990s. Building on previous studies focusing on ‘miniature ice caps’ and other small-sized perennial ice bodies (Haeberli and others, 2004; Bohleber, 2019), Guillet and Ravanel (2020) hypothesized the ice composing ice

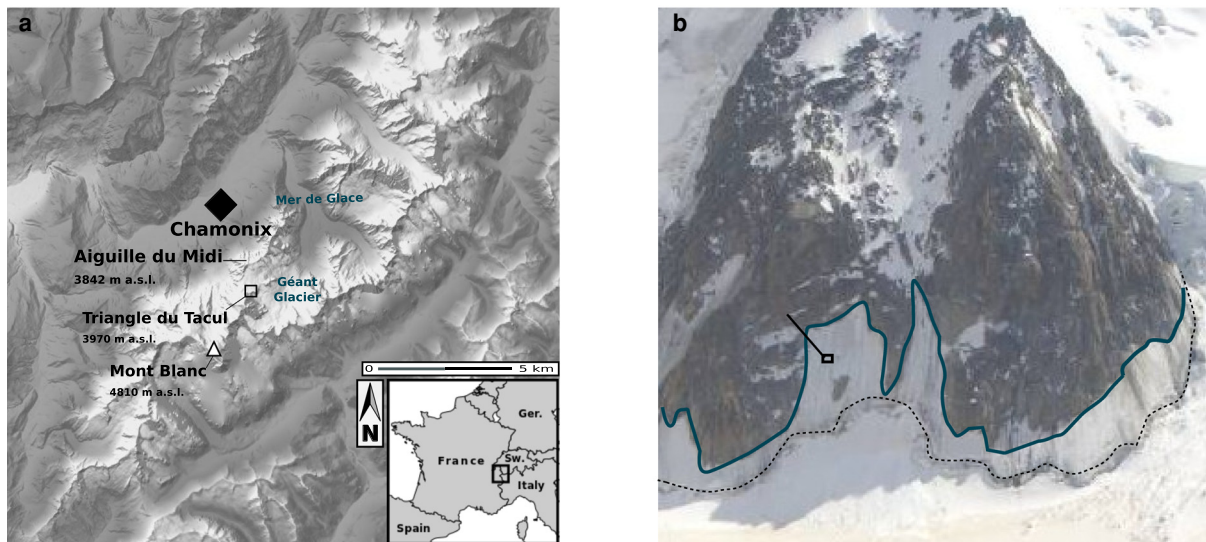


Fig. 1. (a) Localization map of the Chamonix valley and the study site. (b) The TDT (peak at 3970 m a.s.l.), its north face and the ice core drilling site at 3650 m a.s.l.

aprons to be quite old, with no clear insight on the potential age range. To get a better understanding of these particular ice bodies, knowledge about flow dynamics and ice ages in deeper layers, and in particular close to bedrock, is needed. To fill this knowledge gap, texture investigation and radiometric dating, suitable for potential ice ages older than a few hundred years, are considered. Since the pioneering studies of Perutz and others (1939), Kamb (1959) and Gow and Williamson (1976), texture investigations have proven to be a valuable tool in the study of the mechanics driving ice creep and glacier flow in glaciers and ice sheets (see e.g. Hudleston, 1977; Alley, 1988; Duval and others, 2000; Montagnat and others, 2012, 2014). In the following work, texture refers to both microstructure, i.e. size and shape of the ice crystals, and to lattice-preferred orientation (LPO), i.e. the distribution of orientations of the optical axis (c -axis, $\langle 0001 \rangle$) in the analyzed sample. The recent refinement of radiocarbon measurement techniques for microscopic organic material from glacier ice (Uglietti and others, 2016; Hoffmann and others, 2017), and its successful deployment for near-bedrock ice at high-altitude cold Alpine glaciers (Jenk and others, 2009; Hoffmann and others, 2018; Preunkert and others, 2019a) as well as lower altitude cold-based glaciers (Bohleber and others, 2018; Bohleber, 2019) make it a well-suited tool to estimate the age of ice aprons.

In this study we focus on a systematic investigation of a single ice apron in the MBM. To do so, we sampled the lower ice apron of the Triangle du Tacul north face (further denoted as TDT, 3970 m a.s.l.). This specific sampling site was selected since the climb to this ice apron (i.e. the only possibility to access such steep ice spots) is neither very long nor particularly exposed to objective hazards. Also, previous on-site drilling showed that the ice apron was only ~ 1 m thick at the drill site, allowing the extraction of a complete surface-to-bedrock cross section of the ice apron using a portable drill device. In April 2018 and 2019 three ice cores were drilled down to the bedrock and used to investigate the ice texture. Without prior knowledge on the possible age of the ice apron, radiometric dating was used as a first approach.

2. Sampling site and methods

2.1. Sampling site

The ice cores presented in this study originate from the north face of the TDT in the MBM, France (see Figs 1 and 2).

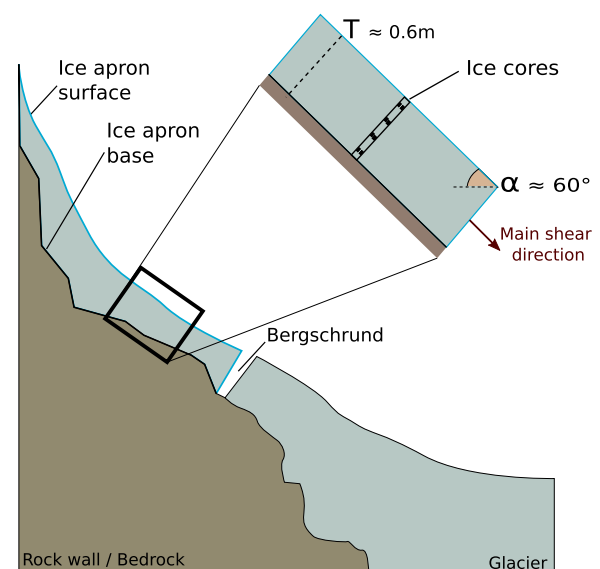


Fig. 2. Schematic representation and geometry of the TDT ice apron.

The mountain face has two distinct ice aprons; only the lower one was sampled. Lying between 3570 and 3690 m a.s.l., it extends over 4000 m² and has a mean slope of $59 \pm 2^\circ$ from horizontal. The retreat of the TDT ice apron since the 1940s has been quantified by Guillet and Ravel (2020). The ice apron has lost close to 20% of its 1940s surface area, with a noticeable increase in the mean melt rate since the 1990s (-10 ± 24 m² a⁻¹ for the 1940–93 period, -46 ± 6 m² a⁻¹ since). Guillet and Ravel (2020) did not note the presence of macroscopic flow features (crevasses or fractures) at the surface of the TDT.

Several drilling campaigns were carried out at the sampling site (close to 3640 m a.s.l.). In March 2017 the ice apron was steam-drilled to bedrock and the 0.6 m-deep borehole, traversing close to 20 cm of seasonal accumulation (fresh snow) and 80 cm of massive ice, was set up for thermal monitoring. The borehole is located close to 3640 m a.s.l. (see Fig. 1). The mean temperature at the ice/rock interface has been measured continuously from March 2017 to April 2019 with an hourly sampling rate. With an annual mean temperature of $-7.6 \pm 4.5^\circ\text{C}$ and all hourly measurements below the melting point, we conclude that the ice apron is still cold and frozen to bedrock. These measurements signal that the



Fig. 3. Coring in the north face of TDT. Core A was drilled where the photographer stands.

underlying bedrock stands under conditions of cold permafrost, and are consistent with the results of previous studies modeling permafrost distribution (Magnin and others, 2015). Furthermore, on-site observations reported no evidence of fractures at the surface of the ice apron, suggesting that circulation of meltwater to the base of the apron is unlikely. In April 2018 and 2019, three 0.6 m-long ice cores (denoted as A, B and C) with a diameter of 5.5 cm were drilled to bedrock within 1 m distance from the 2017 borehole, using a portable drilling system (see Fig. 3) developed by Petzl and the Institut des Géosciences de l'Environnement, for drilling in technical terrain (Montagnat and others, 2010). All three ice cores reached bedrock after 60 cm. Ice thickness measurements made at the 2017 borehole showed that the ice apron lost ~20 cm of thickness between March 2017 and April 2019 at the sampling location. All ice cores were kept at temperatures below -7°C in refrigerated containers before being stored at -25°C in freezers, 4–5 h after their extraction.

2.2. Analytical methods

2.2.1. Texture and LPO

From core B, we produced thin sections covering the entire thickness of the ice apron, in order to study potential changes in the ice texture with depth. Thin sections were made following standard experimental protocols for texture analysis, using bandsaws and a microtome to cut and polish the samples (Schwarz and others, 1981; Durand and others, 2006). Typical thin sections are 9–10 cm long, 4–5 cm wide and 0.4–0.5 mm thick. From the thin sections, LPOs were measured using an automatic ice-texture analyzer (AITA, Russell-Head and Wilson 2001). The AITA provides c -axis orientations over the thin section surface, at a spatial resolution of 20 μm (for this study), together with a quality criterion, enabling the removal of high-uncertainty sample areas, such as grain boundaries (see Peternell and others (2011) for more details).

2.2.2. Particulate organic carbon (POC) content and radiocarbon dating

In the present study, we used a preparation protocol developed by Hoffmann and others (2018) for radiocarbon analysis of POC. This protocol has previously been successfully applied to investigate the age of near-basal ice from cold, high-altitude Alpine



Fig. 4. Lowest part of core A. 12 and 32 cm on the measurement tape correspond to 20 cm above bedrock and the core end, respectively. Note the increase in impurity content between the 22, 27.5 and 30 cm marks (dashed lines).

glaciers (Hoffmann and others, 2018; Preunkert and others, 2019a, 2019b).

Without prior knowledge about the age of ice and the total POC content at the sampling site, we only sampled the deeper layers of cores A and C (core B was used for microstructure investigations, see Section 2.2.1), thus excluding potential bias from near-surface artifacts (Figure 4).

Ice decontamination, melting, filtration, acidification and separation of the bulk organic carbon fraction from the total filtered insoluble carbonaceous particles by combustion at 340°C was done following the approach of Preunkert and others (2019a), using the in-line filtration–oxidation unit REFILOX (Reinigungs-Filtrations-Oxidationssystem (Hoffmann and others, 2018) with mean mass-related combustion efficiency of 0.7 (Hoffmann and others, 2018).

Due to the inevitable tradeoff between the necessary minimum sample mass needed to obtain a sufficient amount of POC ($> 2 \mu\text{g C}$ with error of 3–7% and $> 10 \mu\text{g C}$ with error $< 2\%$) (Hoffmann and others, 2018), and the length (i.e. the time interval covered by each sample), ice cores were cut into 9–20 cm long samples, after removing the outer parts. This resulted in three ice samples with masses of 130–350 g; further reduced to 63–220 g after decontamination by rinsing with ultra-pure water.

After cryogenic extraction of the CO_2 produced from POC combustion, radiocarbon analyses were performed at the accelerator mass spectrometer (AMS) facility at the Curt-Engelhorn-Centre

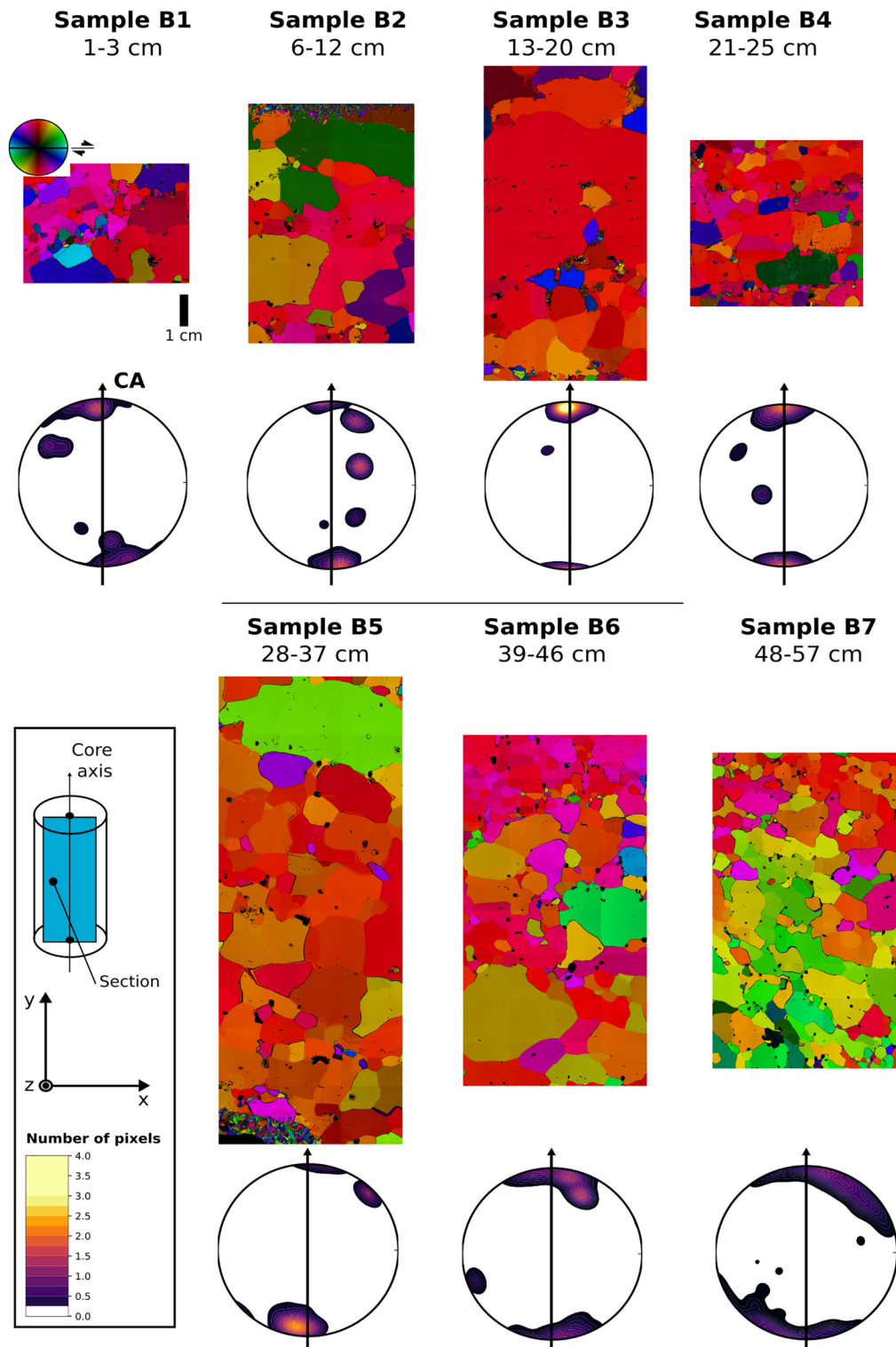


Fig. 5. AITA analyses of thin section for every sample of core B. Color-coded *c*-axis orientation is represented by the color wheel, along with the supposed shear plane. Pole figures (equal area) show the distribution of *c*-axis orientations as well as the core axis (CA). Color scale represents the relative number of pixels plotted. Indicated lengths correspond to depth interval of each sample.

Archaeometry (CEZA, Mannheim, Germany), equipped with a Gas Interface System (GIS, Hoffmann and others 2017).

AMS measured $F^{14}C$ (fraction modern carbon, see Stenström and others (2011); Taylor (1987); Donahue and others (1990) for more details) values were corrected for blank contribution. Hereby, we accounted (1) for the mean $F^{14}C$ blank of the sample set (0.715 ± 0.07) obtained from regularly sampled ultra-pure water blanks ($n = 4$) for which four filters were respectively pooled, due

to the very low carbon content in the blanks, (2) the carbon mass of the ultra-pure water blank determined directly before each sample extraction, ranging from 0.1 to 0.27 $\mu\text{g C}$ (see Preunkert and others (2019a) for further details on the sample preparation procedure).

Calibrated ^{14}C ages were finally obtained using the IntCal13 atmospheric curve (Reimer and others, 2013) OxCal version 4.3 (Bronk Ramsey, 1995, 2009). Calibrated ^{14}C ages are rounded according to Millard (2014).

3. Results and discussion

3.1. Texture and stress state in the TDT ice apron

Microstructure and *c*-axis orientation pole figures (stereographic projections) from seven different depths covering the entire ice core are presented in Figure 5. Although the mean estimated grain size is ~ 1 cm, strong grain size differences can be observed (Fig. 5) within the sections, with some grains being several centimeters wide. We identify irregularly shaped grains, as well as grain boundary bulging and pinning by air bubbles throughout the ice samples (Fig. 6). It should be noted that, owing to the serrated shape of some grains, and the 2-D observation, small grains are the likely result of a protrusion sectioning. The characteristics of the observed microstructures (i.e. large spread in grain sizes, and a 3-D serrated grain boundaries) prevent from providing statistically representative grain size data. Nevertheless, we observe smaller grains the closer the sample is to the bedrock. This type of microstructure is typical of what is expected during deformation at high temperature when dynamic recrystallization is the main accommodating mechanism (Jacka and Maccagnan, 1984; Treverrow and others, 2012). Indeed, dynamic recrystallization is known to induce elongated grains with serrated grain boundaries, owing to strain-induced grain boundary migration driven by the heterogeneously spread stored deformation energy. Dynamic recrystallization also produces bi-modal type of grain size distributions, owing to the small grains resulting from nucleation mechanisms (Montagnat and others, 2009).

LPO, evaluated here with the orientations of the *c*-axes, is represented by means of pole figures (Fig. 5). On all pole figures, we observe *c*-axes preferentially clustered around a direction parallel to the core axis. Apart from the dominant contribution of grains with *c*-axes parallel to the core axis, several tilted grains (green colors in Fig. 5) can be observed throughout the ice core, with more occurrences when getting closer to the bedrock. The LPOs observed along this core are very similar to LPOs documented in some glacier configurations (Hudleston, 1977, 2015) or as a result of laboratory experiments (Bouchez and Duval, 1982; Journaux and others, 2019) and are attributed to the deformation of ice under simple shear associated with the occurrence of dynamic recrystallization as a relaxation mechanism. Typical LPO patterns for ice deformed in simple shear and dynamically recrystallized are composed of two maxima, evolving to a single maximum with increasing strain, oriented normal to the shear plane (Hudleston, 1977; Journaux and others, 2019). The single maximum LPO observed in the TDT ice therefore likely reveals a dominant shear regime, with a shear plane parallel to the surface slope of the ice apron. The inclined (relatively to the core axis) sub-maximum of the observed LPOs in the deeper samples could indicate a lower amount of shear and/or a reduced impact of dynamic recrystallization in the ice located closer to the bedrock. It would be coherent with the fact that the larger grains are observed when getting closer to the surface (samples B3 and B2). Hampering of grain boundary migration related to dynamic recrystallization could be due to pinning by either bubbles or impurities (see Fig. 6), which concentrations have not been evaluated here. From the intensity of the observed LPO, and by comparison with the previous studies mentioned above, we typically estimate the total cumulated shear strain γ to be, at minimum, in the range of $0.5 \leq \gamma \leq 0.8$.

3.2. POC content and radiocarbon dating

By combustion of the filtered carbonaceous aerosols at 340°C, the fraction derived and denoted as organic carbon (OC) is – prior to the time of anthropogenic fossil fuel combustion – originating mainly from direct primary emission of the living biosphere

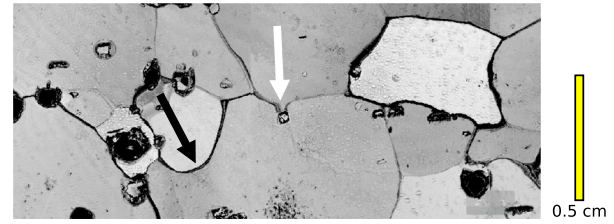


Fig. 6. Close-up of thin section 4 of the TDT ice core. The black arrow indicates a bulging grain boundary while the white arrow highlights grain boundary pinning by an air bubble.

and is therefore well suited for ^{14}C dating (Jenk and others, 2006, 2009; Uglietti and others, 2016; Hoffmann and others, 2018). Although at higher combustion temperatures age biasing is likely to occur due to additional combustion of already aged organic material and remaining carbonates in mineral-dust-rich layers (Jenk and others, 2006), Uglietti and others (2016) achieved to validate the accuracy of ^{14}C dating using the water-insoluble OC fraction combusted at 340°C (here denoted as POC) of carbonaceous particles in ice by a direct comparison of the POC- ^{14}C derived ages with the ages determined independently by other methods (e.g. counting of annual layers) in the same samples of ice.

The resulting POC masses and FC values of the TDT samples after blank correction are given in Table 1. Final POC masses were 13.2 to 33.0 $\mu\text{g C}$, leading to POC concentrations of $330 \pm 140 \text{ ng C g}^{-1}$. These values are nearly 15 times higher than values found in the lowest meters of the neighboring Col du Dome glacier (hereafter denoted CDD), located 5 km southwest of the TDT ice apron, at an altitude of 4250 m a.s.l. (Preunkert and others, 2019b).

The study of atmospheric free cellulose (a proxy for plant debris) in Europe by Sánchez-Ochoa and others (2007), between the altitudes of 0 and 3000 m a.s.l., showed that the annual decrease in mean airborne plant debris with elevation is similar to that observed for SO_4^{2-} during summer. Extrapolating these results via the vertical gradient of atmospheric SO_4^{2-} during summer (Preunkert and others, 2001) to the TDT ice apron and the nearby CDD (i.e. altitudes of 3640 and 4250 m a.s.l.), we expect a difference of a factor 4, which is not enough to explain the apparent difference between the TDT and CDD POC concentrations. To get further information about the origin of the high POC concentration found in the TDT ice, we analyzed major ions from two ice samples (C01 and C02) representing ice from 10–30 cm above bedrock (core C) using ion chromatography (IC; see Preunkert and Legrand (2013) for analytical details). The mean of these two samples was compared to CDD yearly (summer and winter) ice layers dated to originate from the beginning of the 20th century, thus largely free of anthropogenic input (Preunkert and Legrand, 2013). Although the TDT core samples represent just a small portion of the ice apron, their overall ionic composition is likely to provide additional insights. As expected, major inorganic airborne impurities (e.g. SO_4^{2-} , NO_3^-), and non-local (e.g. non-ammonium oxalate components, see below) NH_4^+ , show TDT to CDD concentration ratios between 1.5 and 5, whereas crustal influenced species (e.g. Cl^- , Na^+ , Ca^{2+} , Mg^{2+} , K^+) result in ratios between 20 and 36, demonstrating the influence of the nearby bedrock. In addition to the inorganic composition, the C_2 di-carboxylate (oxalate) was analyzed in the two samples and found to be abundant in the TDT ice, with an enhancement of a factor ≈ 55 compared to the CDD ice of the beginning of the 20th century. Being present most likely as ammonium oxalate this suggests, as demonstrated for the basal layers of the Greenland GRIP ice core (Tison and others, 1998), the existence of considerable deglaciated areas with significant

Table 1. Overview of masses (corrected for blanks but not for combustion efficiency) and ^{14}C ages of the TDT ice core samples combusted in the REFILOX system

Sample name	Depth (cm)	Mass (g)	POC mass ($\mu\text{g C}$)	^{14}C (F^{14}C)	Calibrated ^{14}C date (cal BCE/CE) at 68.2%	Calibrated ^{14}C age range at 68.2% (year cal BP ^a)	Mean calibrated ^{14}C -age (year cal BP ^a)
A-01	32–52	220	32.4	0.725 ± 0.008	830–540 BCE	2780–2490	2640 ± 130
C-01	30–40	96	33.0	0.919 ± 0.008	1270–1390 CE	680–560	630 ± 55
C-02	40–49	63	13.2	0.713 ± 0.012	1080–770 BCE	3030–2720	2840 ± 175

Calibrated date ranges are shown at 68.2% probability and rounded according to Millard (2014). ^a Years before 1950.

plant cover and efficient biological activities in the vicinity of the formation-site of the ice leaving a footprint during the formation of the ice apron.

Ice ages obtained in cores A and C suggest that the ice at depths between ≈ 30 and 50 cm (30–10 cm above bedrock) formed 630–3100 years ago, whereby the two samples from core C indicate an age increase with depth (Table 1).

Considering the small size and steep bedrock slope of the ice apron, a strong increase of ~ 2000 years over such a short interval of 10 cm (core C) might surprise. However the order of magnitude of the age–depth gradient, as well as the absolute ice age 10 cm above bedrock (i.e. ≈ 3000 years) are comparable to those already detected for basal ice in high-altitude cold Alpine glaciers. Basal ice ages were found to be ≈ 4000 cal years BP (gradient of $\approx 40 \text{ a cm}^{-1}$) (Hoffmann and others, 2018) and $>10\,000$ cal years BP (gradient of $\approx 120 \text{ a cm}^{-1}$) (Jenk and others, 2009) for two different ice cores drilled at the high-altitude cold glacier site of Colle Gnifetti (4450 m a.s.l., Monte Rosa region, Switzerland), whereas ice dating ≈ 7000 cal years BP (gradient of $\approx 70 \text{ a cm}^{-1}$) was found for Mount Ortles (3905 m a.s.l., Eastern Alps) (Gabrielli and others, 2016) and for the base of the Piz Murtèl (3433 m a.s.l., Grisons, Swiss Alps) miniature ice cap (Bohleber, 2019). Very recently, near-bedrock ice from an ice core drilled at the CDD was estimated to be $\approx 5600 \pm 600$ year BP (gradient of $\approx 60 \text{ a m}^{-1}$) (Preunkert and others, 2019b). In addition, the occurrence of such old ice is not confined to altitudes ≥ 4000 m a.s.l. Bohleber and others (2018) showed that the lowermost ice layers of the Chli Titlis cold-based glacier (3030 m a.s.l., Central Switzerland) are up to ≈ 5000 years old.

A common feature of the depth–age relationship at the above-mentioned sites and more generally under undisturbed and stable glacier flow conditions, is that the ice becomes older with increasing depth. In addition, due to glaciological flow characteristics both predicted in models (Nye, 1963; Haeberli and others, 2004, among others) and documented by direct measurements (Uglietti and others, 2016), the age gradient with depth becomes strongly enhanced near bedrock. The two stacked samples in core C suggest that the TDT ice also becomes older with depth. Assuming an absence of basal melting during the past (see Section 2.1), and considering a largely regular shear deformation parallel to bedrock as suggested from ice texture investigations (see Section 3.1), we hypothesize the deepest part of the ice is older than the ice age estimated at a depth of 41 ± 11 cm, i.e. older than 3000 years.

3.3. Formation and evolution of the TDT ice apron

Our results showed that the ice composing the TDT ice apron mainly deforms under a low-strain rate simple shear stationary regime and that deformation is rather homogeneous along the axis of the core. Radiocarbon dating results further highlighted an increase in the age of the ice from the surface to the base of the apron, associated with an enhanced age–depth gradient in the lowermost layers ($\approx 2000 \text{ a } 10 \text{ cm}^{-1}$, see Table 1). From our results, it is however not possible to decipher potential past

variations of the ice apron's stress field. Still, further hypotheses can be proposed to explain the formation and evolution of the TDT ice apron.

In most of the cold high-altitude glaciers mentioned in the previous section, the enhanced age–depth gradient in the lowermost layers is a consequence of annual layer thinning. Such thinning results from the strong shear and high strain-rate above the bedrock in cold glaciers frozen to the bed (Uglietti and others, 2016). Although thinning likely also occurs in the ice layers of the TDT apron, we do not believe it to be the main contributor to the observed depth–age gradient. Guillet and Ravel (2020) indeed demonstrated that the main mass balance drivers for ice aprons are climate and the local topography, as only snowfall between -5 and 0°C can accumulate on such steep slopes (Kuroiwa and others, 1967; Guillet and Ravel, 2020). Furthermore, bergschrunds at the foot of ice aprons (see Fig. 1) are widely recognized as separating two different regimes of ice dynamics: (1) the stagnant ice apron (above the bergschrund) and (2) the main flowing glacier (below the bergschrund) (Mair, 1994; Cogley and others, 2011). Building on these considerations and the current study, we hypothesize that the TDT ice apron formed by accumulation and densification of snow into ice and has always been detached from the glacier beneath. We thus believe that the observed variations in the age–depth gradient are more likely to reflect modifications in accumulation rate (and by proxy climate) (Guillet and Ravel, 2020) rather than layer thinning, and to lead to discontinuous depth age profile.

4. Conclusions

In this paper, we presented texture analysis and micro-radiocarbon dating of cores collected on the TDT ice apron. The study of the microstructure and LPO of the ice provided insight into the dynamic behavior of such objects. Similar single maximum LPOs throughout the core indicate simple shear deformation associated with dynamic recrystallization. The transition in LPO and grain size observed closer to the bedrock could likely be the consequence of a lower amount of cumulated shear strain, together with differences in concentrations of impurities and/or air bubbles, trapped while the ice formed. Dynamic recrystallization is the most probable driver for grain growth, producing irregularly shaped grains. Grain-boundary pinning seems to be mainly caused by air bubbles and impurities. Overall similar LPO throughout the ice core signals the lack of recent mass gain by snow accumulation or meltwater refreeze. Micro-radiocarbon measurements indicate that the TDT ice becomes older with increasing depth. We observed ice ages older than 600 year BP and greater than 3000 years in the lowest 30 cm.

The combination of ice dating back to several thousand years with the absence of meltwater influence, makes this kind of small ice body potentially useful as archive for reconstructing the environmental history of Europe. Ice aprons offer the distinct advantage of direct access to a millennial chronology compacted on a few meters of ice, accessible from the surface. However, such records are likely discontinuous and may not allow for trivial

reconstruction of climate history. The potential to serve as an environmental archive still needs to be further demonstrated. Further investigations, preferentially on an ice apron with higher accumulation rates than the TDT to avoid bedrock influence, are therefore needed.

Acknowledgements. This study is part of the ANR 14-CE03-0006 VIP Mont Blanc and the EU ALCOTRA AdaPT Mont Blanc project. We thank Michel Legrand and Owen King for their help and constructive comments during the writing of the manuscript. We thank the Editor as well as W. Haerberli and two anonymous reviewers for their very valuable comments which helped to improve the manuscript significantly.

References

- Alley RB (1988) Fabrics in polar ice sheets: development and prediction. *Science* **240**(4851), 493. doi: [10.1126/science.240.4851.493](https://doi.org/10.1126/science.240.4851.493).
- Armstrong T and Roberts B (1956) Illustrated ice glossary. *Polar Record* **8** (52), 4–12. doi: [10.1017/S0032247400045599](https://doi.org/10.1017/S0032247400045599).
- Barker ML (1982) Traditional landscape and mass tourism in the Alps. *Geographical Review* **72**(4), 395–415. doi: [10.2307/214593](https://doi.org/10.2307/214593).
- Bhutiyan MR (2011) Ice apron. In Singh VP, Singh P and Haritashya UK (eds), *Encyclopedia of Snow, Ice and Glaciers*. Netherlands, Dordrecht: Springer, pp. 581–582, ISBN 978-90-481-2642-2 (doi: [10.1007/978-90-481-2642-2_254](https://doi.org/10.1007/978-90-481-2642-2_254)).
- Bohleber P (2019) Alpine ice Cores as Climate and Environmental Archives. *Oxford Research Encyclopedia of Climate Science*.
- Bohleber P, Hoffmann H, Kerch J, Sold L and Fischer A (2018) Investigating cold based summit glaciers through direct access to the glacier base: a case study constraining the maximum age of Chli Titlis glacier, Switzerland. *The Cryosphere* **12**, 401–412.
- Bouchez J and Duval P (1982) The fabric of polycrystalline ice deformed in simple shear: experiments in torsion, natural deformation and geometrical interpretation. *Texture, Stress, and Microstructure* **5**, 171–190.
- Bronk Ramsey C (1995) Radiocarbon calibration and analysis of stratigraphy: the OxCal program. *Radiocarbon* **37**(2), 425–430. doi: [10.1017/S0033822200030903](https://doi.org/10.1017/S0033822200030903).
- Bronk Ramsey C (2009) Bayesian analysis of radiocarbon dates. *Radiocarbon* **51**(1), 337–360. doi: [10.1017/S0033822200033865](https://doi.org/10.1017/S0033822200033865).
- Cogley JG and 10 others (2011) Glossary of glacier mass balance and related terms. (IHP-VII Technical Documents in Hydrology No. 86, IACS Contribution No. 2) UNESCO–International Hydrological Programme, Paris.
- Deline P and 16 others (2021) Ice loss from glaciers and permafrost and related slope instability in high-mountain regions. In Haerberli W and Whiteman C eds. *Snow and Ice-Related Hazards, Risks and Disasters*, Second Updated Edition, Elsevier edition, 501–540. doi: [10.1016/B978-0-12-817129-5.00015-9](https://doi.org/10.1016/B978-0-12-817129-5.00015-9).
- Donahue DJ, Linick TW and Jull AT (1990) Isotope-ratio and background corrections for accelerator mass spectrometry radiocarbon measurements. *Radiocarbon* **32**(2), 135–142. doi: [10.1017/S0033822200040121](https://doi.org/10.1017/S0033822200040121).
- Durand G and 5 others (2006) Ice microstructure and fabric: an up-to-date approach for measuring textures. *Journal of Glaciology* **52**(179), 619–630. doi: [10.3189/172756506781828377](https://doi.org/10.3189/172756506781828377).
- Duval P, Arnaud L, Brissaud O, Montagnat M, de la Chapelle S (2000) Deformation and recrystallization processes of ice from polar ice sheets. *Annals of Glaciology* **30**, 83–87. doi: [10.3189/172756400781820688](https://doi.org/10.3189/172756400781820688).
- Gabrielli P and 40 others (2016) Age of the Mt. Ortles ice cores, the Tyrolean iceman and glaciation of the highest summit of south Tyrol since the northern hemisphere climatic optimum. *The Cryosphere* **10**(6), 2779–2797. doi: [10.5194/tc-10-2779-2016](https://doi.org/10.5194/tc-10-2779-2016).
- Gow AJ and Williamson T (1976) Rheological implications of the internal structure and crystal fabrics of the West Antarctic ice sheet as revealed by deep core drilling at Byrd station. *GSA Bulletin* **87**(12), 1665–1677. doi: [10.1130/0016-7606\(1976\)87:1665:RIOTIS;2.0.CO;2](https://doi.org/10.1130/0016-7606(1976)87:1665:RIOTIS;2.0.CO;2).
- Gruber S and Haerberli W (2007) Permafrost in steep bedrock slopes and its temperature-related destabilization following climate change. *Journal of Geophysical Research* **112**(F02S18). doi: [10.1029/2006JF000547](https://doi.org/10.1029/2006JF000547).
- Guillet G and Ravel L (2020) Variations in surface area of six ice aprons in the Mont-Blanc massif since the Little Ice Age. *Journal of Glaciology* **66** (259), 777–789. doi: [10.1017/jog.2020.46](https://doi.org/10.1017/jog.2020.46).
- Haerberli W, Frauenfelder R, Kääh A and Wagner S (2004) Characteristics and potential climatic significance of 'miniature ice caps' (crest- and cornice-type low-altitude ice archives). *Journal of Glaciology* **50**(168), 129–136. doi: [10.3189/172756504781830330](https://doi.org/10.3189/172756504781830330).
- Hall PCM and Higham DJ (2005) *Tourism, Recreation and Climate Change*. Bristol, Great-Britain: Channel View Publications.
- Hasler A, Gruber S and Haerberli W (2011) Temperature variability and thermal offset in steep alpine rock and ice faces. *The Cryosphere* **5**(2), 721–753. doi: [10.5194/tc-5-721-2011](https://doi.org/10.5194/tc-5-721-2011).
- Hoffmann H and 6 others (2018) A new sample preparation system for micro-14c dating of glacier ice with a first application to a high alpine ice core from Colle Gnifetti (Switzerland). *Radiocarbon* **60**(2), 517–533. doi: [10.1017/RDC.2017.99](https://doi.org/10.1017/RDC.2017.99).
- Hoffmann H, Friedrich R, Kromer B and Fahrni S (2017) Status report: implementation of gas measurements at the MAMS ¹⁴C AMS facility in Mannheim, Germany. *Nuclear Instruments and Methods in Physics Research Section B: Beam Interactions with Materials and Atoms* **410**, 184–187. doi: [10.1016/j.nimb.2017.08.018](https://doi.org/10.1016/j.nimb.2017.08.018).
- Hudleston PJ (1977) Progressive deformation and development of fabric across zones of shear in glacial ice. In Saxena SK, Bhattacharji S, Annersten H and Stephansson O (eds), *Energetics of Geological Processes: Hans Ramberg on His 60th Birthday*. Berlin Heidelberg, Berlin, Heidelberg: Springer, 121–150, ISBN 978-3-642-86574-9 (doi: [10.1007/978-3-642-86574-9_7](https://doi.org/10.1007/978-3-642-86574-9_7)).
- Hudleston PJ (2015) Structures and fabrics in glacial ice: a review. *Journal of Structural Geology* **81**, 1–27. doi: [10.1016/j.jsg.2015.09.003](https://doi.org/10.1016/j.jsg.2015.09.003).
- Huggel C, Clague JJ and Korup O (2012) Is climate change responsible for changing landslide activity in high mountains?. *Earth Surface Processes and Landforms* **37**(1), 77–91. doi: [10.1002/esp.2223](https://doi.org/10.1002/esp.2223).
- Jacka TH and Maccagnan M (1984) Ice crystallographic and strain rate changes with strain in compression and extension. *Cold Regions Science and Technology* **8**, 269–286. doi: [10.1016/0165-232X\(84\)90058-2](https://doi.org/10.1016/0165-232X(84)90058-2).
- Jenk TM and 7 others (2006) Radiocarbon analysis in an alpine ice core: record of anthropogenic and biogenic contributions to carbonaceous aerosols in the past (1650–1940). *Atmospheric Chemistry and Physics* **6**(12), 5381–5390. doi: [10.5194/acp-6-5381-2006](https://doi.org/10.5194/acp-6-5381-2006).
- Jenk TM and 9 others (2009) A novel radiocarbon dating technique applied to an ice core from the Alps indicating late Pleistocene ages. *Journal of Geophysical Research: Atmospheres* **114**(D14305) doi: [10.1029/2009JD011860](https://doi.org/10.1029/2009JD011860).
- Journaux B and 6 others (2019) Recrystallization processes, microstructure and crystallographic preferred orientation evolution in polycrystalline ice during high-temperature simple shear. *The Cryosphere* **13**(5), 1495–1511. doi: [10.5194/tc-13-1495-2019](https://doi.org/10.5194/tc-13-1495-2019).
- Kamb WB (1959) Ice petrofabric observations from Blue Glacier, Washington, in relation to theory and experiment. *Journal of Geophysical Research* (1896-1977) **64**(11), 1891–1909. doi: [10.1029/JZ064i011p01891](https://doi.org/10.1029/JZ064i011p01891).
- Kenner R and 5 others (2011) Investigation of rock and ice loss in a recently deglaciated mountain rock wall using terrestrial laser scanning: Gemsstock, Swiss Alps. *Cold Regions Science and Technology* **67**(3), 157–164. doi: [10.1016/j.coldregions.2011.04.006](https://doi.org/10.1016/j.coldregions.2011.04.006).
- Kuroiwa D, Mizuno Y and Takeuchi M (1967) Micromeritical properties of snow. *Physics of Snow and Ice* **1**(2), 751–772.
- Magnin F, Deline P, Ravel L, Noetzi J and Pogliotti P (2015) Thermal characteristics of permafrost in the steep alpine rock walls of the Aiguille du Midi (Mont Blanc massif, 3842 m a.s.l.). *The Cryosphere* **9**(1), 109–121. doi: [10.5194/tc-9-109-2015](https://doi.org/10.5194/tc-9-109-2015).
- Mair R and Kuhn M (1994) Temperature and movement measurements at a bergschrund. *Journal of Glaciology* **40**(136), 561–565. doi: [10.3189/S0022143000012442](https://doi.org/10.3189/S0022143000012442).
- Millard AR (2014) Conventions for reporting radiocarbon determinations. *Radiocarbon* **56**(2), 555–559. doi: [10.2458/56.17455](https://doi.org/10.2458/56.17455).
- Montagnat M and 6 others (2010) Waterfall ice: formation, structure and evolution. *Journal of Glaciology* **56**(196), 225–234. doi: [10.3189/002214310791968412](https://doi.org/10.3189/002214310791968412).
- Montagnat M and 6 others (2012) Measurements and numerical simulation of fabric evolution along the Talos Dome ice core, Antarctica. *Earth and Planetary Science Letters* **357–358**, 168–178. doi: [10.1016/j.epsl.2012.09.025](https://doi.org/10.1016/j.epsl.2012.09.025).
- Montagnat M and 11 others (2014) Multiscale modeling of ice deformation behavior. *Journal of Structural Geology* **61**, 78–108. doi: [10.1016/j.jsg.2013.05.002](https://doi.org/10.1016/j.jsg.2013.05.002).
- Montagnat M, Durand G and Duval P (2009) Recrystallization processes in granular ice. *Suppl. Issue Low Temperature Science* **68**, 81–90.
- Mourey J, Marcuzzi M, Ravel L and Pallandre F (2019) Effects of climate change on high alpine mountain environments: evolution of

- mountaineering routes in the Mont Blanc massif (western Alps) over half a century. *Arctic, Antarctic, and Alpine Research* **51**(1), 176–189. doi: [10.1080/15230430.2019.1612216](https://doi.org/10.1080/15230430.2019.1612216).
- Nye JF** (1963) Correction factor for accumulation measured by the thickness of the annual layers in an ice sheet. *Journal of Glaciology* **4**, 785–788.
- Perutz MF, Seligman G and Bragg WH** (1939) A crystallographic investigation of glacier structure and the mechanism of glacier flow. *Proceedings of the Royal Society of London. Series A. Mathematical and Physical Sciences* **172**(950), 335–360. doi: [10.1098/rspa.1939.0108](https://doi.org/10.1098/rspa.1939.0108).
- Peternell M, Russell-Head DS and Wilson CJL** (2011) A technique for recording polycrystalline structure and orientation during in situ deformation cycles of rock analogues using an automated fabric analyser. *Journal of Microscopy* **242**(2), 181–188. doi: [10.1111/j.1365-2818.2010.03456.x](https://doi.org/10.1111/j.1365-2818.2010.03456.x).
- Preunkert S and 5 others** (2019a) The Elbrus (Caucasus, Russia) ice core glaciochemistry to reconstruct anthropogenic emissions in central Europe: the case of sulfate. *Atmospheric Chemistry and Physics* **19**, 14119–14132. doi: [10.5194/acp-19-14119-2019](https://doi.org/10.5194/acp-19-14119-2019).
- Preunkert S and 9 others** (2019b) Lead and antimony in basal ice from Col du Dôme (French Alps) dated with radiocarbon: a record of pollution during antiquity. *Geophysical Research Letters* **46**(9), 4953–4961. doi: [10.1029/2019GL082641](https://doi.org/10.1029/2019GL082641).
- Preunkert S and Legrand M** (2013) Towards a quasi-complete reconstruction of past atmospheric aerosol load and composition (organic and inorganic) over Europe since 1920 inferred from alpine ice cores. *Climate of the Past* **9**(4), 1403–1416. doi: [10.5194/cp-9-1403-2013](https://doi.org/10.5194/cp-9-1403-2013).
- Preunkert S, Legrand M and Wagenbach D** (2001) Sulfate trends in a Col du Dôme (French Alps) ice core: a record of anthropogenic sulfate levels in the European midtroposphere over the twentieth century. *Journal of Geophysical Research: Atmospheres* **106**(D23), 31991–32004. doi: [10.1029/2001JD000792](https://doi.org/10.1029/2001JD000792).
- Ravanel L, Deline P, Lambiel C and Vincent C** (2013) Instability of a high alpine rock ridge: the lower Arête des Cosmiques, Mont Blanc massif, France. *Geografiska Annaler: Series A, Physical Geography* **95**(1), 51–66. doi: [10.1111/geoa.12000](https://doi.org/10.1111/geoa.12000).
- Reimer PJ and 29 others** (2013) Intcal13 and marine13 radiocarbon age calibration curves 0–50000 years cal BP. *Radiocarbon* **55**(4), 1869–1887. doi: [10.2458/azu_js_rc.55.16947](https://doi.org/10.2458/azu_js_rc.55.16947).
- Russell-Head D and Wilson C** (2001) Automated fabric analyser system for quartz and ice. In *Geological Society of Australia Abstracts*, volume 64, 159–159, Geological Society of Australia; 1999.
- Sánchez-Ochoa A and 5 others** (2007) Concentration of atmospheric cellulose: a proxy for plant debris across a west-east transect over Europe. *Journal of Geophysical Research: Atmospheres* **112**(D23S08). doi: [10.1029/2006JD008180](https://doi.org/10.1029/2006JD008180).
- Schwarz J and 7 others** (1981) Standardized testing methods for measuring mechanical properties of ice. *Cold Regions Science and Technology* **4**(3), 245–253. doi: [10.1016/0165-232X\(81\)90007-0](https://doi.org/10.1016/0165-232X(81)90007-0).
- Stenström K, Skog G, Georgiadou E, Genberg J and Mellström A** (2011) *A guide to radiocarbon units and calculations*. LUNFD6(NFFR-3111)/1-17/ (2011), Lund University, Nuclear Physics.
- Taylor R** (1987) Preface. In Taylor R ed. *Radiocarbon dating an archaeological perspective*. London, United Kingdom: Academic Press, pp. ix–x, ISBN 978-0-12-684860-1. doi: [10.1016/B978-0-12-684860-1.50004-0](https://doi.org/10.1016/B978-0-12-684860-1.50004-0).
- Tison JL and 5 others** (1998) Is a periglacial biota responsible for enhanced dielectric response in basal ice from the Greenland Ice Core project ice core? *Journal of Geophysical Research: Atmospheres* **103**(D15), 18885–18894. doi: [10.1029/98JD01107](https://doi.org/10.1029/98JD01107).
- Treverrow A, Budd WF, Jacka TH and Warner RC** (2012) The tertiary creep of polycrystalline ice: experimental evidence for stress-dependent levels of strain-rate enhancement. *Journal of Glaciology* **58**(208), 301–314. doi: [10.3189/2012JogG11J149](https://doi.org/10.3189/2012JogG11J149).
- Uglietti C and 6 others** (2016) Radiocarbon dating of glacier ice: overview, optimisation, validation and potential. *The Cryosphere* **10**, 3091–3105. doi: [10.5194/tc-10-3091-2016](https://doi.org/10.5194/tc-10-3091-2016).